Supplementary materials for Dual-stage structural response to quenching charge order in magnetite

Wei Wang[1,*], Junjie Li[1], Lijun Wu[1], Jennifer Sears[1], Fuhao Ji[2], Xiaozhe Shen[2], Alex H. Reid[2], Jing Tao[1,#], Ian K. Robinson[1,3], Yimei Zhu[1,*], Mark P. M. Dean[1,*]

[1]Condensed Matter Physics and Materials Science Division, Brookhaven National Laboratory, Upton, NY 11973, USA
[2]SLAC National Accelerator Laboratory, Menlo Park, CA 94025, USA
[3]London Centre for Nanotechnology, University College, London WC1E 6BT, UK
[#]Current address: Department of physics, University of Science and Technology of China, 230026 Hefei, Anhui, China

I. Electronic resistance measurement

The resistance as a function of temperature measured from magnetite sample is shown in Fig. S1. There is a sharp increase in the resistance at 115 K, indicating the transition temperature. The electron diffraction taken at 89 K, which is below 115 K, shows multiple superlattice reflections, indicating the structural transition from cubic phase to monoclinic phase. The changes shown in the electronic structure and crystal lattice demonstrate the high-quality single crystal.
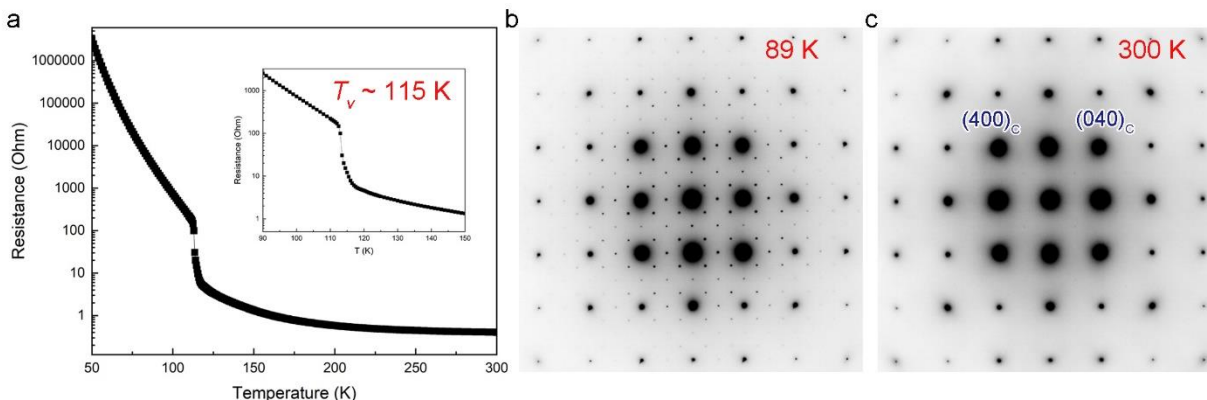
Fig. S1. Verwey transition in magnetite sample. **a** Resistance measurement as a function of temperature. The insert is the enlarge view of the data near the phase transition temperature [1]. **b**, **c** electron diffraction pattern along [001] orientation at 89 K and 300 K, respectively.

II. Electron diffraction simulation

In the electron diffraction simulation, sample bending effect is considered using electron-beam precession. The simulated electron diffraction patterns without and with beam precession are shown in Fig. S2. In Fig. S2b, the intensity of the high-order Bragg peaks reduces quickly. Comparing the simulated reflection intensities with the experimental UED pattern, the simulated pattern with precession angle 1.5° is closer to experimental result.
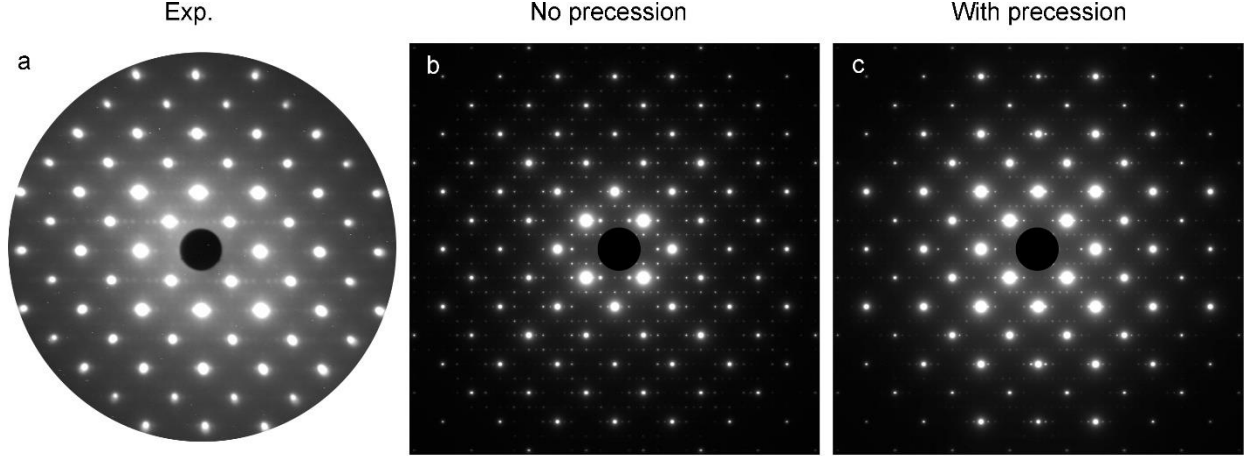
Fig. S2. Experimental diffraction pattern and simulated diffraction patterns. **a** Experimental diffraction pattern taken at t = 0 ps. **b, c** Simulated diffraction pattern without and with precession angle.

III. Averaged SL intensity measurement results
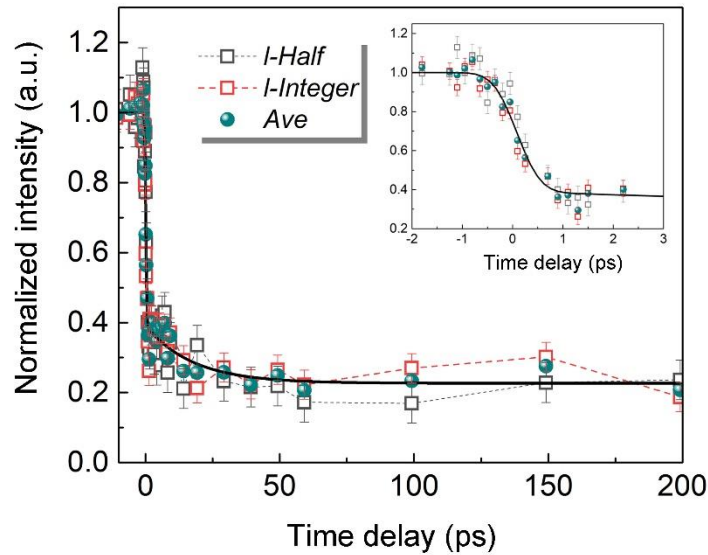
FIG. S3. The SL reflections measurement results. The red square is the data measured from the SL reflections with (h, k, l = half-integers); the grey square is the data measured from the SL reflections with (h, k, l = integers). The blue spheres are the averaged intensity variation of total 32 SL reflections in a long timescale. The intensity drops fast in the first 0.7 ps, then changes slowly and the intensity becomes flat after 100 ps. The black line is fitting result from the averaged data and is for the eye guide.

IV. Simulated results based on Δ_4, X_4, W_1, W_2 modes

Electron diffraction patterns were simulated using the lattice distortion models following Δ_4, X_4, W_1, W_2 modes. The corresponding intensity difference maps are shown in Fig. S3, which are not

consistent with the experimental observations. Therefore, we conclude that these phonon modes are not the dominant driving forces for the lattice distortion.
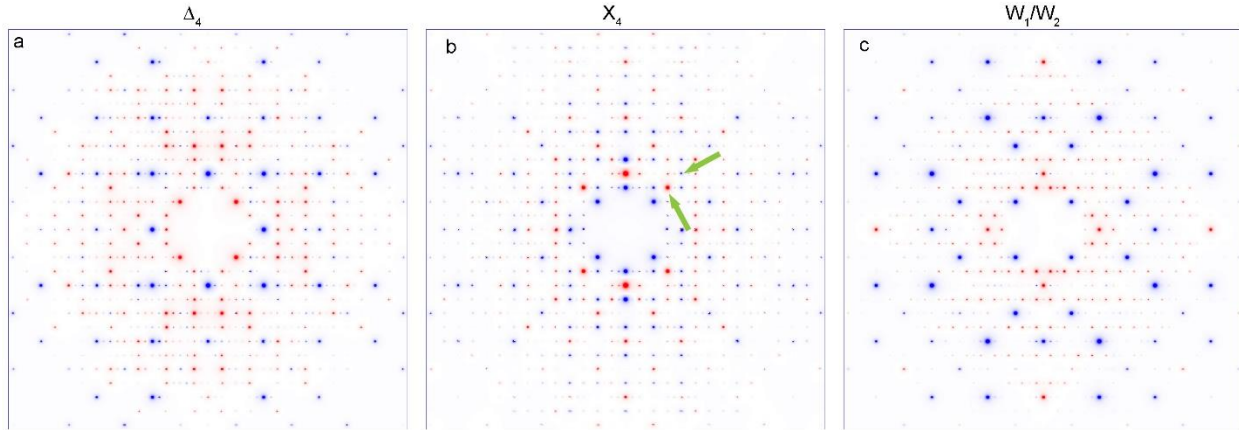
Fig. S4. a-c Simulated intensity difference map based on Δ_4, X_4, W_1, W_2 modes. The green arrows in **b** pointed out the incompatible intensity variations, compared with the result based on the X_3 mode. The intensity different maps induced by W_1, W_2 -type lattice distortion are similar shown in **c**.

V. Intensity difference maps at 3 mJ·cm^{-2} and 7.5 mJ·cm^{-2}
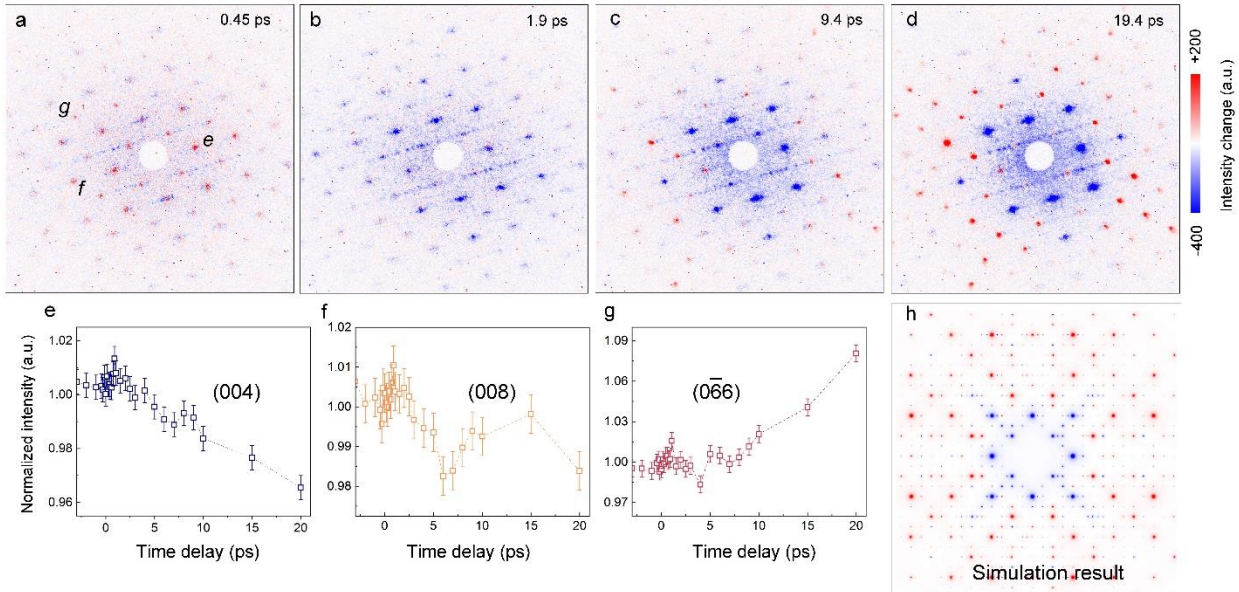
FIG. S5. Intensity changes at different time delays at 3 mJ·cm^{-2}. **a-d** Intensity difference map at a few representative time delays. **e-g** Intensity as a function of time measured from three Bragg peaks. The peak positions in the diffraction pattern are labeled in **a**. **h** Simulated intensity different map for 19.4 ps. In the simulation model, there are only *x-y* atomic displacements following the Δ_5 phonon modes, as shown in Table IV, $\delta_2 = 0$. $\delta_1 = 0.006$ in the simulation.

3
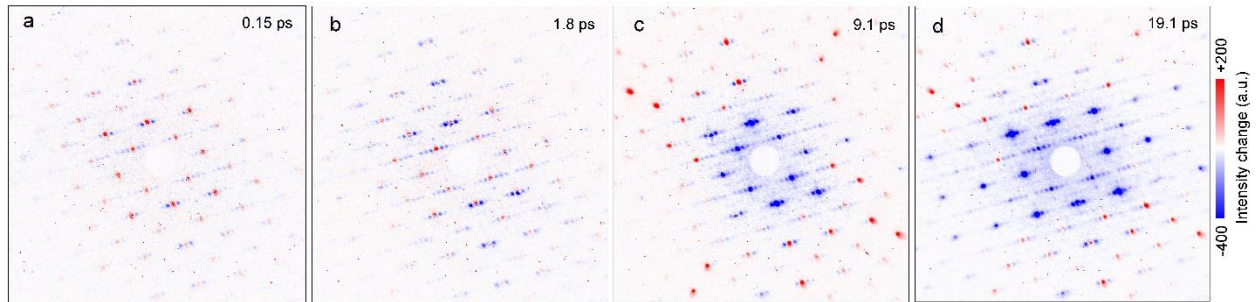
Fig. S6. Intensity changes at different time delays at 7.5 mJ·cm^{-2}.

References

[1] W. Wang, J. Li, Z. Liang, L. Wu, P. M. Lozano, A. C. Komarek, X. Shen, A. H. Reid, X. Wang, Q. Li, et al., *Verwey Transition as Evolution from Electronic Nematicity to Trimerons via Electron-Phonon Coupling*, ArXiv220208744 Cond-Mat (2022).